Analyst

RSC Publishing

PAPER

View Article Online
View Journal | View Issue

Cite this: *Analyst*, 2013, **138**, 6127

Exploring the speed limits of liquid chromatography using shear-driven flows through 45 and 85 nm deep nano-channels

Selm De Bruyne,[ab] Wim De Malsche,*[ab] Veronika Fekete,[a] Hugo Thienpont,[c] Heidi Ottevaere,[c] Han Gardeniers[b] and Gert Desmet[a]

Received 28th May 2013
Accepted 18th July 2013

DOI: 10.1039/c3an01325a

www.rsc.org/analyst

We explored the possibility to perform high speed and high efficiency liquid chromatographic separations in channels with a sub-100 nm depth. The mobile phase flow through these nano-channels was generated using the shear-driven flow principle to generate high speed flows which were the equivalent of a 12 000 bar pressure-driven flow. It was found that the ultra-fast mass transfer kinetics prevailing in this range of small channel depths allow to drastically reduce the C-term contribution to band broadening, at least up to the upper speed limit of our current set-up (7 mm s^{-1} mobile phase velocity), leaving the inescapable molecular diffusion (*i.e.*, B-term band broadening) as the sole detectable source of band broadening. Due to the greatly reduced mass transfer limitations, 50 000 to 100 000 theoretical plates could be generated in the span of 1 to 1.5 seconds. This is nearly two orders of magnitude faster than the best performing commercial pressure-driven UHPLC-systems. With the employed channel depths, we appear to have struck a practical lower limit for the channel miniaturization of shear-driven flows. Despite the use of channel substrates with the highest grades of optical flatness, the overall substrate waviness (on the order of some 5 to 10 nm) can no longer be neglected compared to the etched channel depth, which in turn significantly influenced the local retention factor and band broadening.

1 Introduction

The separation resolution in liquid chromatography (LC) has basically two enemies: longitudinal molecular diffusion and mass transfer resistance.[1] Whereas the first one is inescapable and is a consequence of the intrinsic molecular diffusion of the analytes, the second one can in principle be completely eliminated by shrinking the distance that needs to be covered by the analytes when exchanging between the mobile and the stationary zone. In open-tubular LC, this distance is determined by the capillary or micro-channel diameter. Mathematically, the beneficial effect of reduction of the channel size for an open-tubular system directly follows from the following general plate height expression for open-tubular LC:[1–4]

$$H = 2\frac{D_m}{u_m} + f_1(k')u_m\frac{{d_{channel}}^2}{D_m} + f_2(k')u_m\frac{{d_s}^2}{D_S} \quad (1)$$

wherein the first term represents the longitudinal molecular diffusion, and the second and the third term respectively represent the mass transfer resistance in the mobile and the stationary zone.

Eqn (1) indeed shows that a thorough miniaturization of the channel diameter $d_{channel}$ and the stationary phase layer thickness d_s can eventually make the second and the third term vanishingly small compared to the first term. To eliminate the mass transfer limitations in liquid chromatography, where the molecular diffusion rates are typically (depending on the type of mobile phase and analyte) five orders of magnitude smaller than in gas chromatography, channels with characteristic dimensions in the nanometer range are needed.[5–9] Recent explorations of the nano or extended nano-space have, amongst others, been made by Kitamori *et al.*[10–12] and Wirth *et al.*[13–15] Without any doubt, the most extreme form of miniaturization has very recently been realized by Singhal *et al.*[16] They demonstrated that even a single template-grown carbon nanotube can be used as a separation column to separate attoliter mixtures of fluorescent dyes. The employed columns were 40 μm long, and were only 70 to 200 nm in outer diameter and 60 to 190 nm in inner diameter.

Whereas these groups used pressure forces to propagate the mobile phase, the separations conducted in the present study make use of the shear-driven flow (SDF) principle[17–29] (see Fig. 1). To apply this principle, a flow channel is needed that consists of two independently movable parts, further referred to as the top and the bottom plate. Pressing both parts against

[a]*Vrije Universiteit Brussel, Department of Chemical Engineering, Pleinlaan 2, 1050 Brussels, Belgium. E-mail: wdemalsc@vub.ac.be; Fax: +32 (0)2 629 32 48; Tel: +32 (0)2 629 33 18*

[b]*MESA+ Research Institute, University of Twente, Enschede, The Netherlands*

[c]*Vrije Universiteit Brussel, Department of Applied Physics and Photonics, Pleinlaan 2, 1050 Brussels, Belgium*

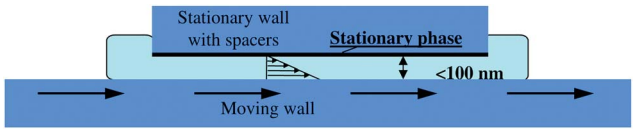

Fig. 1 Working principle and resulting flow profile of a shear-driven flow (SDF). The retentive layer needed for the chromatographic separation is attached to the stationary wall.

each other while moving the top plate past the bottom plate, or *vice versa*, the drag forces originating from the moving plate literally drag the liquid through the channel, as they generate a fluid flow (having a linear velocity profile) that is mechanically sustained all along the channel length.

Since the driving force for the flow is imposed all along the channel length and not only at the channel entrance, as is the case in pressure-driven flow systems, the liquid does not experience any pressure drop at all. Whereas the average fluid velocity in a pressure-driven flow inevitably decreases with increasing channel length and decreasing channel depth (*cf.* Poiseuille's law[30]) for an imposed maximal pressure, the average fluid velocity in a shear-driven flow through a channel with a flat-rectangular cross-section (with width $\gg$ depth) is always equal to one half of the moving wall velocity, completely independent of the channel depth or length.[17,18,23] As a consequence, high speed flows (on the order of cm s^{-1} and more) can easily be imposed in channels with a nanometric depth. The only limitation is the speed of the motorized translation or rotation stage used to drive the moving wall. The channel depth, which is determined by the thickness of the gap formed between the stationary and the moving wall, is maintained by firmly pressing both channel parts against each other and using a set of spacer structures which are micro-machined on either the stationary or the moving wall to form a fixed gap size (=effective channel height, see Fig. 2a). To induce the actual separation, the stationary wall should be coated with a suitable retentive layer (*e.g.*, a layer of C18-alkyl chains).[17]

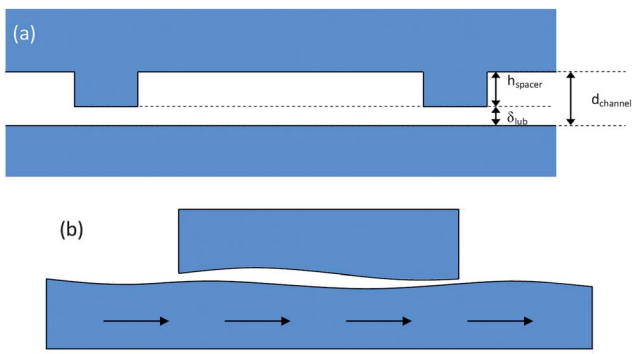

Fig. 2 (a) Schematic cross-sectional view of an SDF channel (cross-section perpendicular to the channel axis; not to scale) showing the stationary wall (top) and the moving wall (bottom) part, the channel spacers (machined into the stationary wall) and the thickness (δ_{lub}) of the lubrication layer underneath the channel spacers. (b) Schematic longitudinal cross-section of the channel showing the large-scale waviness of the substrates (not to scale).

Until now, the shallowest channels wherein the SDF principle has been successfully applied were 120 nm deep.[25] In these channels, plate heights as low as 0.25 μm have been reported, with plate generation velocities on the order of 39 000–52 000 plates per second.

In the present study, we report for the very first time on the use of sub-100 nm channels (45 and 85 nm). For the specific case of SDFs, the main challenge arising when entering this range of channel depths is finding channel substrates which are sufficiently flat to guarantee that the effective channel height is sufficiently reproducible and uniform in space and time. This is due to the fact that the effective channel depth ($d_{channel}$) of SDF channels equals the sum of the etched spacer height (h_{spacer}) and the thickness of the lubrication layer (δ_{lub}) covering the top of the spacers (see Fig. 2a). The thickness of the latter is difficult to control: whereas the layer is initially relatively thick, typically of the order of a few hundreds of nanometers, it continuously decreases (first rapidly, then slowly) under the action of the normal load that is applied to keep the two channel plates in intimate contact. Theoretical considerations show that, under the action of a constant load, the thickness of the excess liquid layer can be expected to decrease according to the square root of the time until the layer becomes so thin that the viscosity starts to increase dramatically because of the decreased mobility of the molecules. According to Israelachvili[31] and Gee *et al.*[32] this occurs when the layer thickness becomes thinner than 5 nm. The thinning of the liquid layer however continues even under these conditions, implying that the application of SDFs inevitably always occurs under conditions of a variable effective channel height.

The only possibility to escape from this problem is by waiting until the lubrication liquid layer has thinned to a value that is sufficiently small so that it no longer contributes significantly to the total effective channel height (total effective channel height = etched spacer height + thickness of the lubrication layer). In this way, the effect of the ever (albeit very slowly) decreasing lubrication layer thickness on the effective channel depth becomes insignificant. In previous experiments, using 100 to 400 nm deep channels,[25,27] it was found that a wait time of 1 minute was sufficient to achieve this, even though the channel spacers had a width of 500–700 μm. This relatively large spacer width, initially selected as such for stability reasons, suffers from the fact that the out-flowing excess liquid needs to travel a relatively large lateral distance. Since the outflow is pressure-driven (originating from the action of the normal load), it is obvious to expect that, the larger the distance that needs to be travelled (*i.e.*, the wider the channel spacer), the slower the outflow velocity of the lubrication layer will be. Considering that the lubrication layer for a channel with a nominal depth of the order of 40 to 80 nm needs to be made as thin as 2 to 4 nm before its contribution to the total effective channel height drops below 5%, it was anticipated that the wait time needed to achieve this would become impractically long. The spacers used in the present study therefore only had a width of 20 μm. To enhance the stability of the stationary wall plate and to keep the local material wear rates as low as possible, the reduction of the individual width of the spacers was compensated by increasing their number (see Fig. 3a).

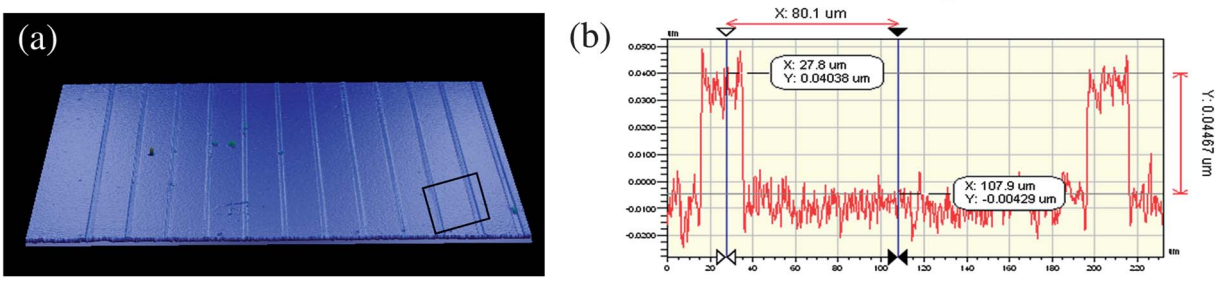

Fig. 3 (a) 3-D Wyko-scan of one of the employed stationary wall plates carrying the half-open SDF-channels. (b) Zoom-in of (a): 2-D Wyko-scan of the surface height profile of the stationary wall substrate, showing two protruding spacer regions having a height of 44 nm (not to scale).

Since the device easily overloads (because of the monolayer stationary phase), and to avoid any influence of the finite time needed for the adsorption and desorption (an effect which increases with the second power of the retention factor) we have chosen to perform the separation of a slightly retained component only.[33] Because of the very low retention factors used in the present study, the experiments could be conducted in a mode wherein the contribution arising from the slow adsorption and desorption times is still negligible. In shear-driven chromatography, this effect is proportional to the square of the retention factor, largely compromising the separation efficiency in the ultra-thin nano-channels for strongly retained components.[33]

2 Experimental

Chemicals and samples

The fluorescent dyes Rhodamine 110 (Exiton Inc., Dayton, Ohio, USA) and Rhodamine 575 (Fluka Chemie GmbH, Buchs, Germany) were used as the analytes in the chromatographic separations. The mobile phase was always a mixture of 50 vol% methanol (LC-MS grade, Biosolve BV, Valkenswaard, The Netherlands) with deionized water.

Microfabrication

The stationary wall parts carrying the channel spacer lines were machined in an ultra-flat optical fused silica wafer (1 mm thick, flatness = $\lambda/20$ with λ = 670 nm, diameter of 4 in., Photox Optical Systems, Sheffield, UK). First, mid-UV lithography (mask aligner: EVG 620, EV Group, St. Florian am Inn, Austria) was used to define the spacers in a positive resist layer (Olin 906-12, Arch Chemicals inc, Zwijndrecht, Belgium) with a thickness of 1.2 μm, spun (spinner Delta 20, SÜSS MicroTec, Garching, Germany) on the wafer surface. After developing the resist (OPD4262, FujiFilm, Japan), the pattern was transferred into the fused silica by deep reactive ion etching (Adixen Alcatel AMS100DE, France). Subsequently, the resist was removed using an oxygen plasma etcher (Tepla 300E, PVA TePla AG, Wettenberg, Germany) and a nitric acid dip (Selectipur: Merck 100453, Germany). Finally, the wafers were diced into chips (Disco DAD321 dicing saw, Japan). Each chip had eight parallel channels with a width of 160 μm and separated by continuous spacer lines of 20 μm width. After their fabrication, the channel wall parts were inspected by making surface height profiles and 3-dimensional profiles using a Wyko NT2000 (Veeco, New York, USA) with a 50× objective and a field of view of 0.5, resulting in an overall magnification of 25×. The C_{18}-stationary phase layer needed to induce the chromatographic retention was induced by silanizing the hydroxyl groups occupying the surface of the half open nanochannels with dimethyloctadecylchlorosilane using the protocol described in ref. 24.

Channel assembly and detection

The main components of the employed set-up have been described in great detail in previous publications.[23,27,28] In brief, the set-up consisted of an inverted epi-fluorescence microscope (IX71, Olympus, Japan) equipped with a mercury vapor lamp (Nikon HB 101-AF, Cetec NV, Belgium) and a high speed EM CCD-camera (electron multiplying charge coupled device camera, Hamamatsu Photonics K.K., Japan) for detection. The movable wall substrate is fixed on the microscope table using a metallic frame holder built in-house. This table could be mechanically moved and positioned using a motorized translation stage (M-TS100DC.5, Newport B.V., The Netherlands), driven by a stepping motor (U611CC, Newport B.V.) and a speed controller (MM 4006, Newport B.V.).

The SDF nano-channels were assembled by putting the diced chip used as the stationary wall inside a precision-milled metal holding frame attached to the microscope head on top of an ultra-flat movable wall substrate (1 mm thick, flatness = $\lambda/20$ with λ = 670 nm, diameter of 2 in., Photox Optical Systems, Sheffield, UK). During the motion, the moving and the stationary part were pressed together using a pneumatic cylinder (PUN-6X1-BL, Festo Belgium NV), positioned directly above the stationary wall plate and contacting it indirectly through a metallic/silicon rubber stack. This force (arising from a typical applied pressure of 1 to 2 bar) is mainly needed to keep both channel parts in close contact and to overcome the natural warp that is present in every unstrained polished material.[24]

Band broadening measurements

Similar to the procedures already described elsewhere,[24,26,27] band broadening was measured by abruptly stopping the wall movement after this has elapsed a preset distance in order to acquire images with good resolution and S/N ratio. The camera

was operated in 8 × 8 binning mode with a 10× objective (OFR LMU-10x-266, Applied Laser Technology, The Netherlands) yielding a pixel size of 11.75 μm. The binning size was chosen as the maximum (8 × 8) in order to achieve the lowest possible capture times to minimize the influence of diffusion after the moving wall stopped abruptly. The band broadening (σ^2) and positions (L_{eff}) of the peaks were quantified by analyzing the recorded data using the SigmaPlot software package (Systat software, Richmond, CA, USA) and fitting the peak intensity profiles with a Gaussian curve function with a given spatial peak variance σ^2. Using the classical plate height definition, the measured variances were first corrected by subtracting the contribution of the injection peak width[19,34] ($H_{\text{inj}} = w_{\text{inj}}^2/12L_{\text{eff}}$) and were subsequently converted into experimental plate height values using:

$$H = \frac{\sigma^2}{L_{\text{eff}}} - \frac{w_{\text{inj}}^2}{12L_{\text{eff}}} \quad (2)$$

wherein w_{inj} is the half of the axial displacement distance of the movable wall during injection following the injection procedure described by Desmet *et al.*[28] w_{inj} varied between 100 and 120 μm for the experiments conducted in the present work.

3 Results and discussion

Using short etching and long conditioning times on the Adixen DE Bosch-etcher, channel spacers with an average height of respectively 85 nm and 40 nm were obtained (Fig. 3). The cited depth values were obtained after averaging out the average depth profile along 10 equidistant transversal lines covering the entire channel axis. Depth fluctuations along a given line were of the order of 2 nm. The average depth variations between the different measurement lines were of the same order. This high degree of depth uniformity could be achieved due to the very high etching uniformity of the Adixen DE combined with the fact that all the employed channels were cut out of the central 50% region of the employed 4 inch wafers.

As mentioned in the Introduction, the generation of reproducible SDFs requires a proper control over the lubrication liquid layer thickness. A first assessment of this thickness can be made by checking whether there is a significant fluorescence intensity coming from the regions underneath the channel spacers. Using the currently employed injection method, the injected sample always contacts the entire front face of the stationary wall platelet.[26] As a consequence, the (fluorescently labeled) sample is also injected in the lubrication layer. When the lubrication layer is sufficiently thin, the fluorescence signal coming from this layer should be negligible compared to the intensity originating from the actual separation channel. Whereas this could relatively easily be achieved using channels with a nominal depth on the order of 200 nm and more, the CCD-images collected during the present study nearly always revealed a slight presence of fluorescently labeled sample underneath the channel spacer (see Fig. 4). This could not be prevented, not even by respecting very long waiting times, leading to the conclusion that the persistence of a relatively thick lubrication layer is due to the overall waviness of the employed substrate materials (represented schematically in Fig. 2b). This waviness prevents the lubrication layer thickness to decrease below a given minimal value. These wall effects however do not contribute to the band broadening because the side-wall effect is a transient process wherein the corresponding plate height starts from a zero contribution and then rises to its final value after a time equaling several times the time needed to diffuse across the width of the channel.[35] The ultra-short duration of the experiment combined with the very large channel width makes this effect insignificant in the present work.

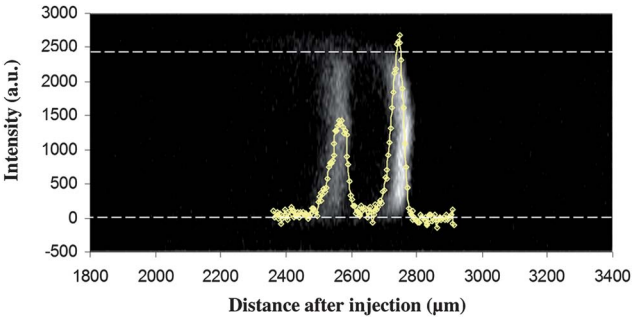

Fig. 4 CCD-camera images of different separations of Rh110 (non-retained peak, $k' = 0$) and Rh575 (slightly retained peak, $k' = 0.07$) in a 45 nm deep channel measured at a mobile phase velocity of 5 mm s^{-1} (corresponding to a moving wall velocity of 10 mm s^{-1}). The effective liquid displacement distance was 2.75 mm. The horizontal dashed lines demarcate the transition between the channel region and the spacers.

A second parameter allowing the assessment of possible differences in the effective channel depth is the effective retention factor k' of the analytes, given by eqn (3).

$$k' = K\frac{V_S}{V_m} = K\frac{\delta_{\text{C18 layer}}}{d_{\text{channel}}} = K\frac{\delta_{\text{C18 layer}}}{(h_{\text{spacer}} + \delta_{\text{lub}})} \quad (3)$$

In this expression, δ_{lub} is the only variable parameter. Eqn (3) shows that, when δ_{lub} is significant compared to the spacer height, any change in its value will also directly contribute to an appreciable change in k'. In the conducted experiments, it was found that k' varied over a value of about 15% when completely repeating the experiment by disassembling the channel to thoroughly clean both channel parts with methanol and a nitrogen gas jet and reassembling the set-up afterwards. Since the 15% repeatability of the k'-factor could not be improved by extending the wait time between the application of the normal load and the start of the separation run, it can be inferred that the run-to-run variations are due to the small differences in the mutual position of the stationary and the moving wall which are inevitable when reassembling the channel. With a spacer height of 45 nm and 85 nm, a change in retention factor of 15% can, according to eqn (3), be calculated to be of the order of some 6 to 12 nm. This is indeed on the same order as the overall surface waviness of the employed channel wall substrates. Despite these substrates having one of the best commercially available flatness values (flatness = $\lambda/20$, with λ = 670 nm), the cited flatness value still implies that the lowest and highest positions on the surface of the moving wall substrate (diameter = 50 mm)

can be expected to have a height difference of the order of 30 nm. As schematically represented in Fig. 2b, the relatively large contact area between the stationary and the moving wall substrate (10 × 20 mm) can, combined with the surface waviness, indeed easily lead to changes in the lubrication layer thickness on the order of a few nanometers and more.

These deviations most probably also explain the variations in band broadening (quantified as the local plate height $H = \Delta\sigma_x^2/\Delta x$ calculated from the difference in spatial variance between two successive axial measurement points) along the channel axis observed in Fig. 5. The represented measurements are taken from a series of subsequent runs with different moving wall travel lengths. The thus imposed effective liquid displacement distances (L_{eff}) ranged from 2.75 to 5.75 mm. For each displacement distance, five consecutive runs were made. As can be noted from Fig. 5, the measured plate heights vary significantly with the elapsed distance (maximal variation on the order of 50% to 100%), while the variation between runs over the same displacement distance is much smaller than the variation between the different displacement distances. The observed pattern is very similar for both analytes (except for the last measurement point), corroborating the hypothesis that the observed variation is directly related to the surface profile of the employed substrates.

The CCD image shown in Fig. 4 respectively corresponds to a separation efficiency of $N = 27\,000$ and $N = 10\,300$ (for Rh110 and Rh575 respectively) for a liquid displacement distance of 2.75 mm (Fig. 4a). The efficiencies obtained at different positions can be deduced from Fig. 5. In terms of plate heights, these efficiencies translate into values of the order of 0.1–0.2 μm for Rh110 and 0.25–0.35 μm for Rh575 (see Fig. 5 for a detailed overview). The highest efficiency value ($N = 99\,000$ plates, corresponding to the $H = 0.06$ μm point at 6.25 mm) was measured for the largest travel distance (6.25 mm). Given that the fluid velocity in this experiment equaled 5 mm s^{-1}, this corresponds to a plate generation velocity of about 77 000 plates per second. We believe this is among the highest values ever reported in the literature for liquid chromatography.

Despite the large variation in plate height observed among the different axial displacement distances, the variability among the values obtained for the same displacement distance is clearly much smaller. This good repeatability also allowed us to measure a full Van Deemter curve to quantify the influence of the imposed liquid velocity on the band broadening, collecting all measurement points at the same axial distance ($L_{eff} = 4$ mm for the data represented in Fig. 6) to rule out the axial variation effect.

At a velocity of $u = 7$ mm s^{-1}, the realized separation efficiency measured for a liquid displacement distance of $L_{eff} = 4$ mm was on the order of $N = 40\,000$ theoretical plates for Rh110 and $N = 20\,000$ for Rh575. At the given speed, this corresponds to a plate generation of 70 000 to 35 000 plates per second. This is more than one order of magnitude faster than is currently achievable with commercial liquid chromatography instruments, where the t_0-times needed to produce 70 000 plates are typically of the order of 1 to 2 minutes (see for example Fig. 7 in Cabooter *et al.*[36]). This corresponds to a plate generation velocity of "only" 1200 plates per s (value cited for a pressure-driven packed bed column operated at 1000 bar). Translating the realized shear-driven flow velocities in the nano-channels into their pressure-driven equivalent, it can be calculated from Poiseuille's law[30] for the pressure-drop in a channel with a flat-rectangular cross-section that a dazzling inlet pressure of 12 000 bar would have been needed in order to achieve the same velocity using the pressure-driven mode in the same 20 mm long and 45 nm deep channel.

The maximal plate generation velocities recorded in the present study are also higher than those obtained by Fekete *et al.*[25] (39 000–52 000 plates per second) in a 120 nm channel. However, the gain is clearly not proportional to the roughly three-fold decrease in channel depth (45 *versus* 120 nm). This smaller-than-expected gain is clearly also related to the fact that no significant difference in separation efficiency can be observed between the two different channel depths (45 and 85 nm) for any of the velocities reported in Fig. 5. Although maybe surprising at first sight, this observation can be entirely explained by theory. Eqn (4) gives one of the explicit variants of

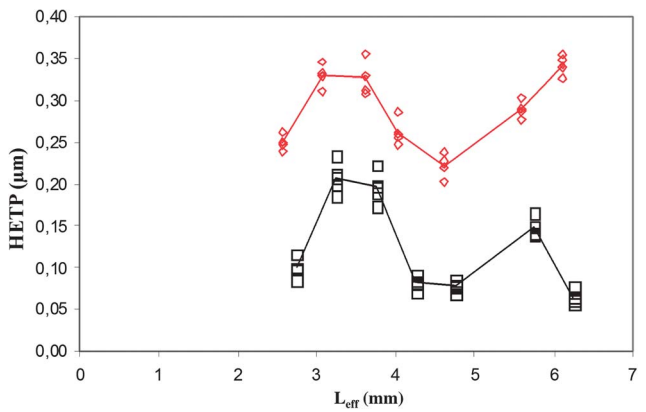

Fig. 5 Plate heights measured at different axial positions in a 45 nm deep SDF-channel (□ Rh110, ◇ Rh575). The full lines connect the averaged values for each series of experiments at different axial positions.

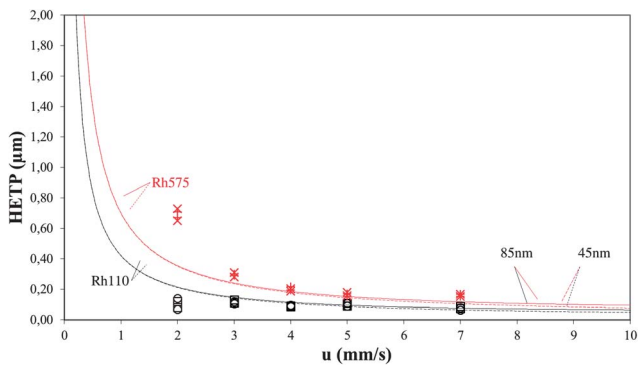

Fig. 6 Experimental plate height values (red and black data points) measured in 45 and 85 nm deep SDF channels compared to the theoretical expectations (85 nm: full lines; 45 nm: dashed lines) determined *via* eqn (4).

eqn (1), wherein the k'-dependency of f_1 and f_2 has been analytically calculated for the flat-rectangular channel cross-section and the linear flow profile of a SDF.[17]

$$H = 2\frac{D_m}{u_m} + \frac{2}{30}\frac{1 + 7k' + 16k'^2}{(1+k')^2}u_m\frac{{d_{channel}}^2}{D_m} + \frac{2}{3}\frac{k'}{(1+k')^2}u_m\frac{{\delta_{C18\ layer}}^2}{D_S} \quad (4)$$

In this equation, the single unknown experimental parameter is the liquid phase diffusion coefficient D_{mol}. To determine this value, a separate series of experiments was conducted in relatively deep ($d = 1.4$ μm), non-coated channels for which it is known from a separate study[29] that the contribution of the wall or stationary phase diffusion coefficient is negligibly small (time spent in the mobile phase $\ggg$ time spent on the surfaces).

The diffusion coefficient experiments were done in the so-called peak parking mode,[37] wherein a band was injected, transported to a given position in the channel where the flow was stopped and the gradual broadening of the band was then recorded *in situ* using the CCD camera. From these measurements, the values for D_{mol} were obtained as one half of the slope of the straight-line relationship between the variation in band broadening ($\Delta\sigma_{band,x}^2$) and the elapsed time interval (Δt). The band diffusion was followed during 60 seconds. An image was captured every 3 s, to minimize the occurrence of photobleaching. The thus obtained values of D_{mol} for the Rh110 and Rh575-species are respectively given by: $D_{mol,Rh110} = (2.1 \pm 0.3) \times 10^{-10}$ m^2 s^{-1} and $D_{mol,Rh575} = (3.5 \pm 0.4) \times 10^{-10}$ m^2 s^{-1}. Using these values in eqn (4), together with the nominal channel depths and the measured k'-values, it is found that the mass transfer distances in the employed nano-channels are indeed so small in the covered range of velocities ($u_m = 1$ to 7 mm s^{-1}) that the band broadening is fully dominated by the molecular diffusion term (first term of eqn (4)). As a consequence, the band broadening has become independent of the channel depth and the theoretical curves for the 40 and 85 nm channels nearly coincide perfectly (Fig. 6, full lines), hence also explaining why the measured plate heights in the 40 and 85 nm channels perfectly coincide with the measurement error margin.

According to eqn (4), a difference in plate height between both channel depths can only be expected at higher mobile velocities ($u_m > 10$ mm s^{-1}), where the mass transfer contribution between the mobile and stationary phase would become significant. Such high velocities are not achievable with the current set-up due to the limited acceleration of the translation stage.

To put the results in a more practical perspective, it should be noted that the very high separation speeds of shear-driven chromatography can, with the present state of detector sensitivity, not be exploited for real-world separations, because of the very small injection and detection volumes, as well as because of the lack of sufficiently long flat substrates enabling the realization of separations with a large retention factor.

4 Conclusions

High speed chromatographic separations have been conducted in nano-channels with two different depths (45 and 85 nm). Using the shear-driven flow principle, velocities as high as 7 mm s^{-1} could be realized. When using the conventional pressure-driven flow principle, this would have required an inlet pressure of about 12 000 bar. Due to the extremely small mass transfer distances (*i.e.*, channel depths), the realized chromatographic separations were devoid of any detectable mass transfer resistance, up to the highest realized velocities. As a consequence, the two different investigated channel depths produced very similar plate height values, fully dominated by the molecular diffusion term of the Van Deemter equation. Under these mass transfer resistance-free conditions, the highest realized separation efficiency was of the order of $N = 50$ to 70 000 theoretical plates per second.

Given the fact that the channels already operate in mass transfer-free conditions, there is no need for a further reduction of the channel depth. This would practically also be very difficult because the surface variations caused by the large scale (long distance) waviness of the employed channel substrates can, despite their high degree of optical flatness (flatness of $\lambda/20$), no longer be neglected compared to the nominal channel depth.

Acknowledgements

W.D.M. gratefully acknowledges Research Foundation-Flanders (FWO Vlaanderen) for a postdoctoral fellowship.

References

1 J. C. Giddings, *Dynamics of Chromatography Part 1*, Marcel Dekker, New York, 1965.
2 M. J. E. Golay, *Gas Chromatography 1958*, ed. D. H. Desty, Butterworths, London, 1958, vol. 36.
3 R. Aris, *Proc. - R. Soc. Edinburgh, Sect. A: Math. Phys. Sci.*, 1959, **252**, 538–550.
4 U. D. Neue, *HPLC Columns*, Wiley-VCH, New York, 1997.
5 L. D. Menard and J. M. Ramsey, *Anal. Chem.*, 2013, **85**, 1146–1153.
6 M. L. Kovarik and S. C. Jacobson, *Anal. Chem.*, 2007, **79**, 1655–1660.
7 M. L. Kovarik and S. C. Jacobson, *Anal. Chem.*, 2009, **81**, 7133–7140.
8 J. P. Kutter, *J. Chromatogr., A*, 2012, **1221**, 72–82.
9 P. Abgrall and N. T. Nguyen, *Anal. Chem.*, 2008, **80**, 2326–2341.
10 K. Mawatari, T. Tsukahara, Y. Sugii and T. Kitamori, *Nanoscale*, 2010, **2**, 1588–1595.
11 M. Kato, M. Inaba, T. Tsukahara, K. Mawatari, A. Hibara and T. Kitamori, *Anal. Chem.*, 2010, **82**, 543–547.
12 R. Ishibashi, K. Mawatari and T. Kitamori, *J. Chromatogr., A*, 2012, **1238**, 152–155.
13 B. Wei, B. J. Rogers and M. J. Wirth, *J. Am. Chem. Soc.*, 2012, **134**, 10780–10782.

14 Z. Zhang, S. N. Ratnayaka and M. J. Wirth, *J. Chromatogr., A*, 2011, **1218**, 7196–7202.
15 B. Wei, D. S. Malkin and M. J. Wirth, *Anal. Chem.*, 2010, **82**, 10216–10221.
16 R. Singhal, V. N. Mochalin, M. R. Lukatskaya, G. Friedman and Y. Gogotsi, *Sci. Rep.*, 2012, **2**, 510.
17 G. Desmet and G. V. Baron, *J. Chromatogr., A*, 1999, **855**, 57–70.
18 G. Desmet and G. V. Baron, *Anal. Chem.*, 2000, **72**, 2160–2165.
19 G. Desmet, N. Vervoort, D. Clicq and G. V. Baron, *J. Chromatogr., A*, 2001, **924**, 111–122.
20 Y. Cai, D. Janasek, J. West, J. Franzke and A. Manz, *Lab Chip*, 2008, **8**(11), 1784–1786.
21 X. Yang, G. Jenkins, J. Franzke and A. Manz, *Lab Chip*, 2005, **5**(7), 764–771.
22 M. S. Anderson, *Anal. Chem.*, 2005, **77**, 2907–2911.
23 D. Clicq, N. Vervoort, R. Vounckx, H. Ottevaere, J. Buijs and G. Desmet, *J. Chromatogr., A*, 2002, **979**, 33–42.
24 V. Fekete, D. Clicq, W. De Malsche, J. G. E. Gardeniers and G. Desmet, *J. Chromatogr., A*, 2007, **1149**, 2–11.
25 V. Fekete, D. Clicq, W. De Malsche, J. G. E. Gardeniers and G. Desmet, *J. Chromatogr., A*, 2008, **1189**, 2–9.
26 D. Clicq, K. Pappaert, S. Vankrunkelsven, N. Vervoort, G. V. Baron and G. Desmet, *Anal. Chem.*, 2004, **76**, 430A–439A.
27 D. Clicq, S. Vankrunkelsven, W. Ranson, C. De Tandt, G. V. Baron and G. Desmet, *Anal. Chim. Acta*, 2004, **507**, 79–86.
28 G. Desmet, N. Vervoort, D. Clicq, P. Gzil, A. Huau and G. V. Baron, *J. Chromatogr., A*, 2002, **948**, 19.
29 K. Pappaert, J. Biesemans, D. Clicq, S. Vankrunkelsven and G. Desmet, *Lab Chip*, 2005, **5**, 1104–1110.
30 H. Schlichting, *Boundary-Layer Theory*, Mc-Graw Hill, London, 1958.
31 J. N. Israelachvili, *J. Colloid Interface Sci.*, 1986, **110**, 263–271.
32 M. L. Gee, P. M. McGuiggan, J. N. Israelachvili and A. M. J. Homola, *Chem. Phys.*, 1990, **93**, 1895–1906.
33 F. Detobel, V. Fekete, W. De Malsche, S. De Bruyne, H. Gardeniers and G. Desmet, *Anal. Bioanal. Chem.*, 2009, **394**, 399–411.
34 H. Poppe, in *Chromatography, fundamentals and applications of chromatograph and related differential migration methods*, ed. E. Heftmann, Journal of Chromatography Library, Elsevier, Amsterdam, 1992, pp. 151–225.
35 K. Broeckhoven and G. Desmet, *J. Chromatogr., A*, 2007, **1172**, 25–39.
36 D. Cabooter, F. Lestremau, F. Lynen, P. Sandra and G. Desmet, *J. Chromatogr., A*, 2008, **1212**, 23–34.
37 A. Liekens, J. Denayer and G. Desmet, *J. Chromatogr., A*, 2011, **1218**, 4406–4416.